RESEARCH PAPER

Influence of Multiple Coating and Heat Treatment Cycles on the Performance of a Nano-TiO_2 Coating in the Protection of 316L Stainless Steel Against Corrosion under UV Illumination and Dark Conditions

M. Karimi Sahnesarayi*, H. Sarpoolaky and S. Rastegari

**karimisahnesara@gmail.com*

Received: April 2018 **Revised: October 2018** **Accepted: January 2019**

[1] School of Metallurgy and Materials Engineering, Iran University of Science & Technology, Iran.

DOI: 10.22068/ijmse.16.2.33

Abstract: *In this study nanosized TiO2 coatings on the 316L stainless steel substrate were prepared by means of dip-coating technique in which thickness of the coating layer increased by repeating the coating cycles in two different routes: (I) dipping and drying, respectively, were repeated one, three and five times and finally the dried coated sample was heat treated (single); (II) multiple heat treatment performed after each dipping and drying cycle, respectively. The structural, morphological and optical characterizations of coatingsthe , as well as the thickness of coatings, were systematically studied. The photocatalytic activity of the various TiO2 coatings was investigated based on the degradation of an aqueous solution of Methyl orange. Moreover, the corrosion protective properties of coatings were evaluated in both dark and UV illumination conditions based on the obtained polarization curves. The results indicated 1.75 times improvement in photocatalytic reaction rate constant, a two orders of magnitude decrease in corrosion current density in dark condition and about 140 mV electrode potential reduction under UV illumination with optimum coating preparation procedure, repeating the cycle from dipping to heat treatment three times, than the sample prepared with one time coating and heat treatment since this procedure provided not only high thickness and defect-free coating but also transparent one.*

Keywords: *Nano-TiO_2 coating, Sol-gel, Stainless steel, Multiple coating and heat treatment cycles, Corrosion protection, Photoelectrochemical cathodic protection.*

1. INTRODUCTION

Stainless steels, particularly 316 stainless steel, are considered as one of the most used materials because of their importance in engineering and wide applicability based on their corrosion behavior. Despite good corrosion resistance of 316 stainless steel in various corrosive environments, it is susceptible to localized corrosion in the presence of chloride ions [1]. Among all reported available treatment methods, modification of stainless steel surface properties by various coating materials is regarded as a suitable method to overcome this problem in terms of effectiveness, economical aspect and easy preparation [2]. Various protective coatings are applied to meet the requirements of corrosion resistance [3-6]. Among these protective coatings, TiO_2 has recently attracted increasing attention as a nanostructured coating because of its ability for photocathodic protection of stainless steel through an extremely promising environment-friendly system. The principle of photocathodic protection provided by the TiO_2 coating has been well known and described obviously in numerous articles [7-9]. The TiO_2 coating as n-type semiconductor converts clean and renewable solar energy (UV illumination) to photo-induced electrons which then are injected to the metal surface, making the electrode potential of the substrate to be more negative than its corrosion potential. Therefore, the TiO_2 coating is known as non-sacrificial photoanode as it does not get consumed in this case. Many investigations were carried out on photocathodic protection of the different substrates, such as carbon steel [10, 11], copper [12] and stainless steel [13-15]. In addition, several studies were reported on the usage of composite coatings by coupling electron storage materials with TiO_2 [16-19] and doped titania coatings [20] in order to modify and improve TiO_2 coatings.

Owing to its fascinating advantages of versa-

[DOI: 10.22068/ijmse.16.2.33]

tility of application, cheap technology and simplicity, sol-gel technique is generally the preferred process to synthesize and deposit metal oxide coatings [21-25]. In previous literatures, intensive efforts have been undertaken to investigate the influence of the various parameters such as corrosive solution conditions (being aerated or non-aerated [26], pH [8, 27], concentration of the corrosive elements [8]), UV light intensity [8] and presence of an intermediate layer between the coating and the substrate [26, 28] on the photocathodic protection performance. Moreover, the most effective heat treatment temperature of sol-gel derived TiO_2 coating was researched in the former study [7].

The thickness of TiO_2 coatings is another notable preparation factor can play a crucial role in the protection ability of TiO_2 coatings as sol-gel coating process usually demonstrates a highly thin coating. To adjust TiO_2 coating thickness, the common method is the utilization of multilayer TiO_2 coating considered as an effective method to improve TiO_2 coating for enhancing photocatalytic activity [29-32]. However, according to our knowledge, there have been few reports in this topic and it persuaded us to examine the effectiveness of multilayer coating in the corrosion protection performance under illumination and dark conditions. For this purpose, our intention was to study the influence of parameters, the number of dipping times and heat treatment times, on the physical properties, anticorrosion and photocatalytic performances.

2. EXPERIMENTAL

2.1. Sol Preparation

Precursor solutions for TiO_2 coatings were prepared by the following method: titanium tetraisopropoxide (TTIP) and diethanolamine (DEA) were dissolved in three-fifths of the total isopropanol (i-PrOH). After the solution was stirred vigorously for 1 h at room temperature, a mixture of water and the rest of i-PrOH was added dropwise within 15 min, under stirring. The solution finally was continuously stirred and aged for 2 h and 48 h, respectively. The relative molar ratio of each chemical in the sol was adjusted to 1:1:25:1 (TTIP : DEA : i-PrOH : W). The flow chart of this method is presented in Fig.1.

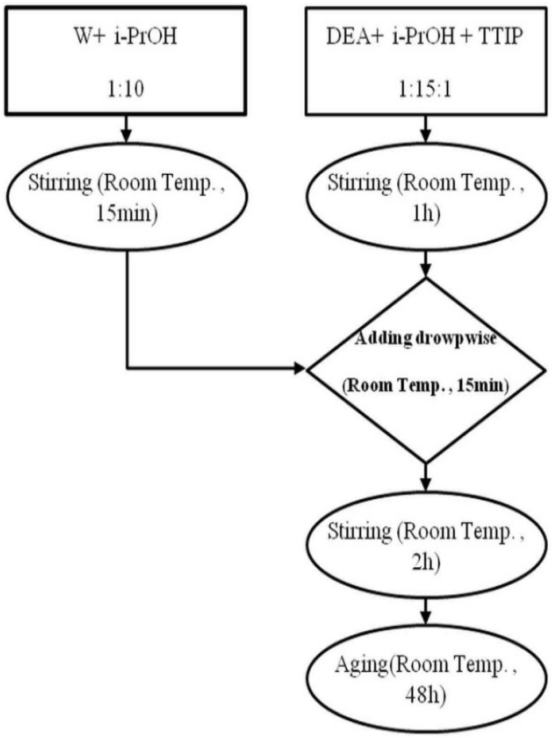

Fig. 1. Schematic processing diagram showing the preparation method of the TiO_2 polymeric sol.

2.2. Substrate Preparation

316L stainless steel sheet with a thickness of 2 mm was used for the preparation of the substrate. After being cut into the size of 10×20 mm^2, the testing side of specimens was ground with No. 80 to 1500 emery papers and was polished to mirror finish using 0.05 µm- and 3 µm-Al_2O_3 particle-included polish solutions. Finally, the specimens were successively sonicated in acetone, ethanol and deionized water each for 10 min, followed by drying in air.

2.3. Sample Preparation

TiO_2 coated stainless steel samples were prepared by dip-coating sol-gel method with the withdrawal speed of 3 cm/min. Then the samples were dried for 2 min at the top region of the sol container before exposure to air to achieve a crack-free TiO_2 coating [33]. It should be noted that different dip-coating and heat treatment cycles were repeated to obtain a thick coating in two methods. In the first method, dipping and drying, respectively, were re-

[DOI: 10.22068/ijmse.16.2.33]

peated one, three and five times and ultimately dried coatings were subjected to a final single heat treatment at an optimum temperature [7], 450 °C for 30 min, with a heating rate of 1 °C/min. However, in the second method, each sample was coated, dried and heat treated, respectively and the procedure was repeated for 1, 3 and 5 times. The heat treatment was performed at 450 °C for 30 min. In the second heat treatment, apart from one or multiple coatings, the heating rate was chosen 1 °C/min (similar to the first method) to avoid crack formation while for subsequent heat treatments the heating rate increased to 5 °C/min. Henceforth for simplicity, the samples will be called according to the number of dipping and heat treatment cycles so that the numbers after D and H letters refer to the number of dipping and heat treatment cycles, respectively; for example, the sample D3H1 specifies the sample was dipped 3 times with single heat treatment.

2.4. Characterization

Phase analysis was carried out based on a grazing incidence X-ray diffraction (GIXRD) using a PANalytical model X'Pert Pro MPD. The incident angle of Cu Kα-radiation was 2° in all measurements.

Microstructures of the TiO_2 coatings were examined using an atomic force microscope (AFM) which was a NanoScope II from Digital Instruments, USA. Non-scraping Si_3N_4 tips were used throughout the examinations by AFM. Also, the film thicknesses were measured using a profilometer (Dektak3, Veeco Inst.)

In order to study the optical behavior of the coatings, quartz samples with dimensions of 20×10×1 mm^3 were prepared in the same way as the coated stainless steel substrates. The transmission spectra of these coatings were measured by a UV-Vis Spectrophotometer Jenway 6705 UV/Vis.

Photocatalytic activities of the prepared TiO_2 coatings were investigated based on the photocatalytic degradation of methyl orange in an aqueous solution. For this measurement, the samples were placed within 10 cm distance from the UV source on a Petri-box containing 30 ml of 10 ppm aqueous solution of methyl orange. The solution pH was adjusted to 3.0 by adding HNO_3. The samples were then irradiated by a UV source (125W, emission spectrum range of 360 – 415 nm) with a maximum intensity of 370 nm (i.e. close to the anatase band gap). The concentration of methyl orange was measured by using a UV–visible spectrophotometer at the wavelength of 505 nm corresponding to the maximum adsorption of methyl orange. Alteration in the concentration of methyl orange was measured in the presence of TiO_2 coating as a function of time.

Photoelectrochemical behaviors of the samples were evaluated in dark and UV illumination conditions using polarization tests by means of an IviumStat potentiostat. A custom made corrosion setup consisted of a platinum counter electrode, a saturated calomel electrode (SCE) as the reference electrode and a bare or coated stainless steel specimen as the working electrode. In addition, corrosion setup was equipped with a quartz glass window on one side for the passage of UV radiation and samples were fixed on the opposite side. In fact, UV radiation was then made to fall on the coated side of the samples after this radiation passed through a quartz window. The test solution was a 3.5 wt.% NaCl solution while the area of the specimen exposed to test solution was maintained at 1 cm^2. In order to simulate the ambient atmosphere, the measurements were carried out under aerated conditions. Firstly, each sample was soaked in the solution for 30 min, and then the polarization curves were obtained by potential sweeps started from the resting potential with a scanning rate of 1 mV/s.

3. RESULTS AND DISCUSSION

3.1 Coated Sample Characterization

3.1.1 Thickness

A thickness analyzer was used to evaluate the thickness of the prepared coatings. The influence of thickness on dipping and heat treatment cycles has been investigated. The coating thickness results are listed in Table1 for the samples prepared at different circumstances.

Table 1. Coating thickness of the samples.

	D1H1	D3H1	D5H1	D3H3	D5H5
Thickness(nm)	198	382	570	592	950

[DOI: 10.22068/ijmse.16.2.33]

The thickness of the D1H1 sample was about 200 nm. Generally, the thickness of the prepared coatings increased as the number of dipping cycles rose so that for single treated samples the average coating thickness per cycle is roughly estimated around 100 nm while this is about 200 nm for the multiple-heat treated samples. The average thickness difference is considered to be due to the fact that the TiO_2 coating cannot be stabilized well before heat treatment, so in each dipping cycle Titania sol replaced and leached a part of the coating deposited in the earlier dipping cycle in the case of D3H1 and D5H1 samples while for the multiple-heat treated samples after each dipping and heat treatment cycle the well-stabilized coating formed on the surface of the samples.

3.1.2 Phase Analysis

The GIXRD diffraction patterns of the samples are shown in Fig.2. It is evident from GIXRD patterns that the heat treated coatings were polycrystalline showing a peak at 2θ =25.4º corresponding to (1 0 1) reflections of the anatase phase of TiO_2. The anatase phase was predominant structure of all the coatings and it is consistent with the previous study in the range from 350 to 500 °C with a very small amount of rutile phase being formed at 500 °C [7]. Consequently, the characteristic peak of rutile isn't observed in D1H1, D5H1, and D3H3 samples. Nevertheless, the X-ray diffraction pattern of the D5H5 sample shows a peak associated with the rutile phase. Therefore increment of heat treatment times and coating thickness led to the transformation of anatase to rutile phase.

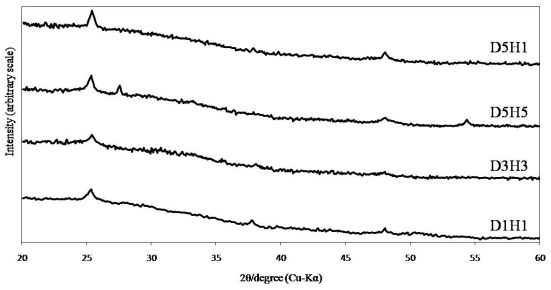

Fig. 2. Grazing incidence x-ray diffraction measurements of TiO_2 coated samples.

3.1.3 Surface Morphological Study

AFM was employed to study the effect of the number of dipping and heat treatment times on the structural and textural characteristics of the sol-gel derived coatings. Fig.3 shows three dimensional surface plots of AFM micrographs taken at the sample surface of coatings prepared by different conditions. Additionally, the nanoscale roughness values of the coatings are given in Table 2.

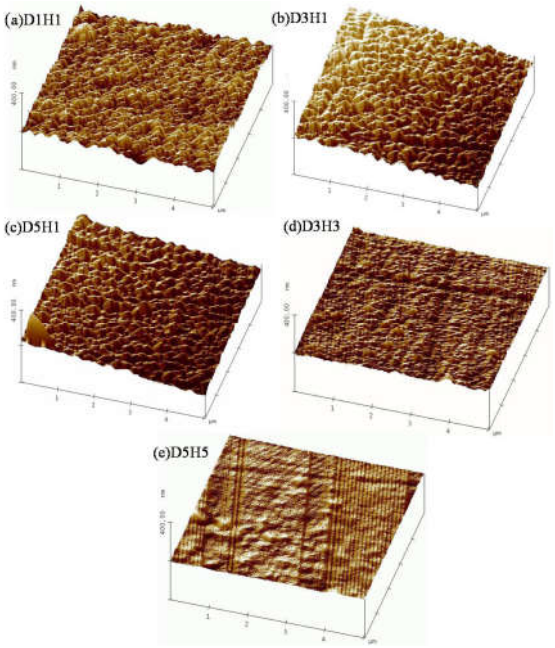

Fig. 3. AFM micrographs of the coatings
(a) D1H1 (b) D3H1 (c) D5H1 (d) D3H3 (e) D5H5.

As can be seen in Fig. 3, uniformly continuous surface textures can be observed for all the samples. The AFM images (Fig.3 a-c) show that the surface structure of the TiO_2 coated samples were not appreciably changed by performing single heat treatment after all dipping and drying cycles. These specimens exhibit nearly uniform coating with mono-dispersed regularly-shaped grains with about 45 nm in diameter. These coatings were made up of interconnected particles and pores, building up high "mountains" and deep "valleys". Their roughness was situated about

Table 2. Surface roughness of the coatings.

	D1H1	D3H1	D5H1	D3H3	D5H5
Surface roughness (nm)	8.58	7.95	8.03	3.57	1.32

[DOI: 10.22068/ijmse.16.2.33]

8.58, 7.9 and 8.0 nm forD1H1, D3H1 and D5H1, respectively. It can be concluded that repeating the dipping cycle didn't have an enormous impact on TiO_2 coating roughness along with the textural characteristic of coatings. This can be attributed to the fact that the nano-titania coating was stabilized well after heat treatment, so the repeating dipping cycle does not have any influence on the feature of the surface before the stabilization of the TiO_2 coating.

On the other hand, it is clearly seen that the morphology of the coatings was greatly changed in multiple-heat treated specimens. The roughness of 3.6 and 1.3 nm was obtained for D3H3 and D5H5 samples, respectively. In fact, by an increment of the cycle from dipping to heat treatment, continuous coating with a smoother morphology was obtained on the stainless steel substrate. This phenomenon was more accentuated for the D5H5 (Fig. 3e). It suggested that the valleys of a coating layer were filled by the next dipping cycle and stabilized by the following heat treatment. Consequently, the surface of coatings became smoother as the cycle from dipping to heat treatment was repeated.

3.1.4 Optical Properties

As UV-Vis spectroscopy offers a convenient method to estimate the approximated electronic band gap. UV–Vis spectra of the TiO_2 coating samples prepared in the different dip-coating cycles were measured and are illustrated in Fig. 4. The optical transmittance spectra of the coatings include two different regions. In the first region of the transmission spectra, interference oscillations which are due to multiple reflections at the coating/substrate and the coating/air interfaces confirm the excellent surface quality and homogeneity of the coatings [34].The optical transmittance spectra of the coatings exhibit good transmission in the visible region and a sharp fall in the UV region as second region. The sharp drop was because of the electronic transition between the valence and conduction bands of titania. In the case of D5H5 specimen, the transmittance of TiO_2 coating diminished, which can be attributed to absorption resulting from the phase transformation from anatase to rutile [35] and higher coating thickness. Actually, thicker TiO_2 coating absorbed more spectrum and decreased the passage of irra-

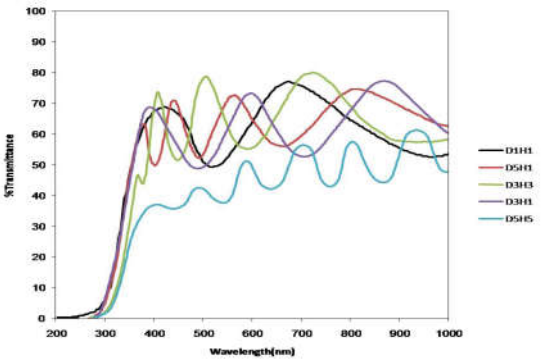

Fig. 4. Optical transmission spectra of TiO_2 coatings.

UV–Vis transmittance spectra showed that absorption edge shifted to longer wavelength in the multiple-heat treated samples (D3H3, D5H5) than the single-heat treated samples (D1H1, D3H1, and D5H1). The same observation also was reported in other literature and was ascribed to the difference in crystallite size. It was believed that coating which undergoes repeated heat treatment cycle contains relatively large crystallites and shows red-shift [29].

3.2. Photocatalytic Activity

The photocatalytic activity of all samples was investigated using the degradation of aqueous methyl orange solution as a model pollutant. The methyl orange photodecomposition profiles as a function of UV illumination exposure time, calculated using equation 1, are shown in Fig. 5.

$$Degradation\ percentage = (C_0\text{-}C)/C_0 \times 100 \quad (1)$$

Where C and $C_0$are the reactant concentration at time t = t and t = 0, respectively.

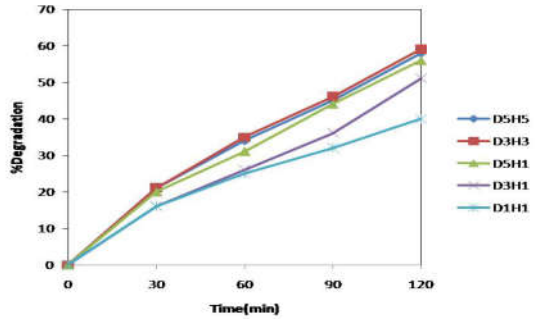

Fig. 5. Methyl orange degradation percentage versus UV illumination exposure time.

[DOI: 10.22068/ijmse.16.2.33]

Methyl orange degradation is clearly observed in Fig. 5 for all samples, indicating that photocatalytic reaction occurred on TiO_2 surface while UV illumination exposes to the nano-titania coating. Indeed, electrons in electron-filled valence band were excited by UV illumination to the conduction band, leaving positive holes in the valence band. These electrons and positive holes drove the reduction and oxidation, respectively, of compounds adsorbed on the surface of a photocatalyst [36]. The dependence of the degradation rate can be described according to the Langmuir-Hinshelwood relationship. This is a very simple but reasonable model in describing our photocatalytic reaction:

$$\mathrm{Ln}\left(\frac{C0}{C}\right)=kt \quad (2)$$

Where k is the apparent rate constant and t stands for time. By plotting $\mathrm{Ln}(C_0/C)$ versus t, the apparent rate constant (k) can be determined from the slope of the curve. Table 3 summarizes the apparent rate constants for all samples.

The increase in photocatalytic degradation efficiency could generally be attributed to two main parameters, surface roughness, and coating thickness. Since the photocatalytic reaction took place at the surface of a semiconductor, with increasing surface roughness the coating surface area increased, followed by enhancement of photodegradation efficiency [36, 37]. Additionally, It is believed that the higher reaction rate constant of the thick TiO_2 coatings closely related to the greater number of electron-hole pairs which generated on the surface of thicker coating because the absorption of photons by the TiO_2 coating rises with the increased thickness[38, 39].

In single-heat treated samples, the increment of the apparent rate constant can be ascribed to the increased thickness while roughness parameter has an insignificant effect on photocatalytic efficiency because of the similar surface roughness of the single-heat treated samples. On the other hand, roughness and thickness are considered as effective parameters in multi-heat treated samples. The photocatalytic activity rose by increasing thickness from D1H1 to D3H3 and D5H5 specimens, as well as the roughness reduction from D3H3 to D5H5, led to lower photocatalytic degradation. Moreover, the translucence and the light scattering increment in the D5H5 sample could lead to a decrease in the irradiation passage through the coating, followed by the reduction of photocatalytic activity. It should be noted that owing to increment of the apparent rate constant from D1H1 to D3H3, the increased thickness is more dominant parameter than reduced roughness in a comparison between D3H3 and D1H1 specimens.

3.3. Corrosion Protection

To determine the corrosion resistance performance of the coatings, polarization tests were carried out in a 3.5 wt.% NaCl solution. Fig. 6 shows the polarization curves for all samples in the dark condition (without UV illumination) and the polarization curve obtained for the uncoated 316L stainless steel. All coated samples presented a typical passivation behavior, in which the current density decreased and maintained nat a low value over a wide potential range. Generally, the passive current density is an important parameter to assess the kinetics of corrosion reaction in specimens and it is normally proportional to the corrosion rate. The numerical values of passive current density (I_{pass}) and corrosion potential (E_{corr}) for each coated specimen and bare stainless steel are shown in Table 4.

Comparison of these curves reveals that by application of TiO_2 coating on stainless steel substrates

Table 3. The constant value regarding the photocatalytic apparent reaction rate for the samples.

	D1H1	D3H1	D5H1	D3H3	D5H5
Rate constant ($\times 10^{-5}$)	411	566	666	721	699

Table 4. Electrochemical corrosion parameters obtained from the polarization curves shown in Figure 6.

	bare	D1H1	D3H1	D5H1	D3H3	D5H5
E_{corr} (mV)	-171	-98	-73	-134	-33	-110
I_{pass} ($\mu A.cm^{-2}$)	477	29.1	3.38	229	0.77	18.6

[DOI: 10.22068/ijmse.16.2.33]

the polarization curves were shifted to the left (lower corrosion current density) and more positive potentials with respect to the uncoated samples. The passivation current density of the coated samples decreased about one to three orders of magnitude compared to the bare steel. The significant reduction in corrosion current density implies that the nano-titania coatings could help to decrease the corrosion rate and increases the chemical resistance of the stainless steel. Furthermore, shifting the corrosion potentials for the coated samples to the positive direction indicated that the entirely shielding TiO_2 coating prevented the surface from attack of anions from the corrosive media to the stainless steel surface and consequently kept the metal in a more stable state in dark conditions.

In the single-heat treated samples, by the increase of the dipping cycle to 3 times (D3H1), i_{corr} decreases by nearly 100 times. It is noted that D3H1 demonstrates a lower i_{corr} than the D1H1, D5H1, and bare stainless steel. However, when five layers are applied (D5H1), higher passive current density and cathodic shift of corrosion potential were obtained, indicating that the corrosion resistance deteriorated. Fig. 7 presents the SEM micrograph of D3H1 and D5H1 samples. In the case of D3H1, a crack-free coating with excellent surface quality and the uniform thickness was prepared as it can be obviously seen from Fig. 7a. Therefore this coating can be considered as an effective barrier to prevent the diffusion of a corrosive element to the substrate. Nevertheless, applying the 5 times-dipping cycle on the stainless steel resulted in the significant changes in surface morphology so that the surface of D5H1 sample contained some crack defects as shown in Fig. 7b. It is believed that the thicker coatings are more prone to crack than thinner ones because the residual stress, which is produced by removal of residual hydroxyl groups and organic compounds as well as induced by thermal expansion mismatch between substrate and coating, can be promoted in heat treatment stage [40]. Thus lower corrosion resistance of D5H1 than D3H1 can be explained as the localized corrosion took place due to defects in the D5H1 sample coating. These results are well congruous with the results achieved by G.X. Shen et al. [27] and J. Masalskiet al. [41], and confirm that raising the dipping cycle to the optimum value provides improved corrosion resistance, while the corrosion resistance declines at dipping cycle higher than the optimum one.

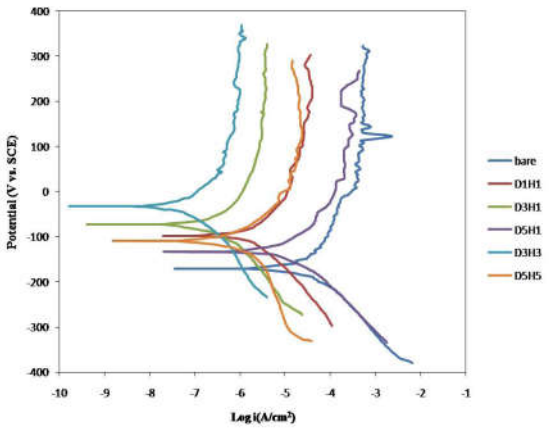

Fig. 6. Polarization curves recorded for the bare 316L stainless steel and the TiO_2-coated 316L stainless steels prepared by different dip-coating conditions (without UV illumination).

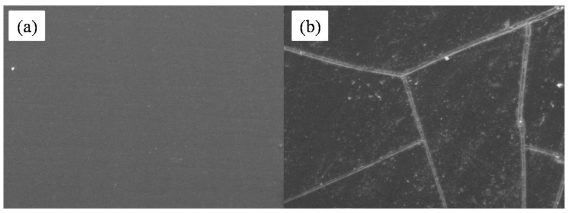

Fig.7. SEM micrograph of the TiO_2 coatings on 316L stainless steel: (a) D3H1 (b) D5H1.

In the case of the multiple-heat treated specimens, increase in the coating cycle up to 3 times resulted in a decrease in passive current density and showed an increase in the corrosion potential, while further increase beyond 3 times coating revealed a reversed trend so that D3H3 demonstrated the best corrosion resistance performance. Additionally, it should be mentioned that D3H3 acted as a better anticorrosion barrier compared to D3H1 due to not only thicker TiO_2 coating but also smoother surface [37].

Polarization curves of the heat treated specimens obtained after 30 min illumination are shown in Fig. 8. It is obvious that the corrosion potentials of the samples examined under UV irradiation were shifted toward negative values and their corrosion-current densities increased. This phenomenon was observed in other papers [26, 27, 42]. When stainless steel coated with TiO_2 was under UV irradiation, the photogenerated electrons in TiO_2 coating were injected into

[DOI: 10.22068/ijmse.16.2.33]

the underlying substrate. Thus they increased the anodic current of the TiO_2-coated 316L stainless steel electrode under UV illumination and drove the potential of the metal shift toward the more negative direction than its corrosion potential and adjust it in the corrosion immunity region. In that case, the corrosion prevention of metals known as photogenerated cathodic protection was achieved and the nano-TiO_2 coating played the role of a non-sacrificial electrode.

As discussed above, the photon absorption of the Titania coating increases with rising its thickness, followed by more electron-hole pairs production [38, 39]. Thus it shifts the electrode potential towards a more negative direction. This fact can be observed in Table 5. It is found that the photo-potential value was more negative with the increased film thickness apart from D5H5. On photocathodic protection ground, more negative potentials or larger corrosion-current densities are regarded as a leading role to achieve appropriate protection [26, 27]. The D3H3 specimen demonstrated the least noble potential and the greatest corrosion-current density in the UV illumination test, indicating that this sample had the most photocathodic protection performance among all the samples tested in this condition. It should be mentioned that electron-hole pairs production diminished in D5H5 sample although it had the thickest coating, owing to the fact that its opacity decreased the amount of absorbed photon. Furthermore, the D5H5 contained not only anatase but also the rutile phase. Consequently, the photoactivity of this sample decreased as a result of the fact that the rutile phase has not proper photoactivity compared to anatase [43].

Because there is the same mechanism in the photocathodic protection and photocatalytic phenomena, i.e. the generation of electron-hole pairs, there is good agreement between these results. Finally, the sample involved three times of coating cycle repetition, from dipping to heat treatment, proved to be the most efficient coating cycle in order to apply both in dark and UV illumination conditions.

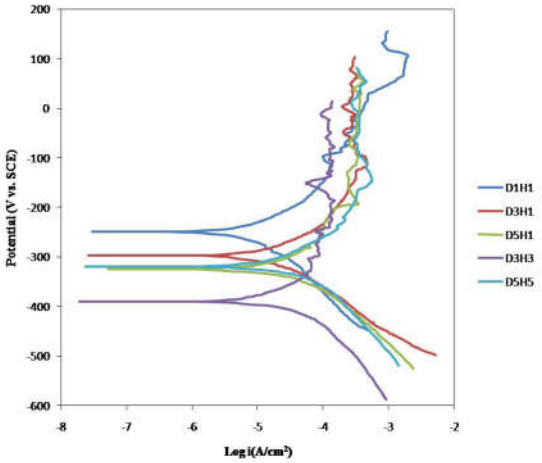

Fig. 8. Polarization curves recorded for the bare 316L stainless steel and the TiO_2-coated 316L stainless steels prepared by different dip-coating conditions (under UV illumination).

4. CONCLUSION

The X-ray diffraction pattern confirmed that although the single-heat treated samples demonstrated pure anatase phase regardless of film thickness, crystallinity in TiO_2 coatings was affected by repeated heat treatment so that D5H5 contained rutile coupled with the anatase phase. Moreover, coating thickness increment led to transparency reduction. The roughness of multiple-heat treated samples decreased while this parameter remained constant in single-heat treated samples by increasing the dipping cycle time. In addition, the photocatalytic degradation activity seemed to generally be proportional to the thickness, aside from the circumstance that the thick TiO_2 coating avoided the irradiation passage through the coating by light scattering.

In the case of corrosion study, the nano-TiO_2 coated 316L stainless steels were cathodically protected from corrosion. These tended to be the most functional when prepared by repeating the cycle from dipping to heat treatment three times which could provide a highly effective chemical resistance in both UV illumination and dark conditions

Table 5. Electrode potential of samples under UV illumination.

	bare	D1H1	D3H1	D5H1	D3H3	D5H5
E_{corr} (mV)	-171	-249	-297	-325	-387	-320

[DOI: 10.22068/ijmse.16.2.33]

due to not only its high thickness and defect-free coating but also its proper transparency nature.

REFERENCES

1. A. International, A.I.A.P.D. Committee, A.I.H. Committee, ASM Handbook, ASM International, 2005, 54-81.
2. Ghali, E. and Sastri, V. S., "Corrosion Prevention and Protection: Practical Solutions," Wiley, 2007 , 90-100.
3. Khorram, M. R., Shishesaz, M. R., Danaee, I. and Zaarei, D., "Synthesis and corrosion protection behavior of epoxyTiO_2-micaceous iron oxide nano - Composite coating on st-37," Iranian Journal of Materials Science and Engineering, 2016, 13, 11-20.
4. Nouri, E., Shahmiri, M., Rezaie, H. R. and Talayian, F., "Investigation of structural evolution and electrochemical behaviour of zirconia thin films on the 316L stainless steel substrate formed via sol–gel process," Surface and Coatings Technology 2011, 205, 5109-5115.
5. Pan, C., Liu, L., Li, Y., Zhang, B. and Wang, F., "The electrochemical corrosion behavior of nanocrystalline 304 stainless steel prepared by magnetron sputtering," Journal of The Electrochemical Society, 2012, 159, C453-C460.
6. García, M. A. L. and Smit, M. A., "Study of electrodeposited polypyrrole coatings for the corrosion protection of stainless steel bipolar plates for the PEM fuel cell, Journal of Power Sources, 2006, 158, 397-402.
7. Karimi Sahnesarayi, M., Sarpoolaky, H. and Rastegari, S., "Effect of heat treatment temperature on the performance of nano-TiO_2 coating in protecting 316L stainless steel against corrosion under UV illumination and dark conditions," Surface and Coatings Technology, 2014, 258, 861-870.
8. Ohko, Y., Saitoh, S., Tatsuma, T. and Fujishima, A., "Photoelectrochemical Anticorrosion and Self-Cleaning Effects of a TiO_2 Coating for Type 304 Stainless Steel," Journal of The Electrochemical Society, 2001, 148, 24-28.
9. Yuan, J., Fujisawa, R. and Tsujikawa, S., "Photopotentials of Copper Coated with TiO_2 by Sol-Gel Method, Zairyo-to-Kankyo, 1994, 43, 433-440.
10. Ren, J., Qian, B., Li, J., Song, Z., Hao, L. and Shi, J., "Highly efficient polypyrrole sensitized TiO_2 nanotube films for photocathodic protection of Q235 carbon steel," Corrosion Science, 2016, 111, 596-601.
11. Deng, H., Huang, M. C., Weng, W. H. and Lin, J. C., "Photocathodic protection of iron oxide nanotube arrays fabricated on carbon steel," Surface and Coatings Technology, 2015, 266, 183-187.
12. Subasri, R. and Shinohara, T., "Photoelectrochemical characterization of TiO2 coatings derived from commercial sol solution for cathodic protection applications, Res Chem Intermediat, 2005, 31, 275-283.
13. Barati, N., Faghihi Sani, M. A. and Ghasemi, H., "Photocathodic protection of 316L stainless steel by coating of anatase nanoparticles," Prot Met Phys Chem Surf, 2013, 49, 109-112.
14. Liu, W., Du, T., Ru, Q., Zuo, S., Cai, Y. and Yao, C., "Preparation of graphene/WO3/TiO_2 composite and its photocathodic protection performance for 304 stainless steel," Materials Research Bulletin, 2018, 102, 399-405.
15. Techapiesancharoenkij, R., Sripianem, W., Tongpul, K., Peamjharean, C., Wichean, T. N., Meesak, T. and Eiamchai, P., "Investigation of the photocathodic protection of a transparent ZnO coating on an AISI type 304 stainless steel in a 3% NaCl solution," Surface and Coatings Technology, 2017, 320, 97-102.
16. Wang, X. T., Wei, Q. Y., Li, J. R., Li, H., Zhang, Q. X. and Ge, S. S. "Preparation of $NiSe_2$/TiO_2 nanocomposite for photocathodic protection of stainless steel," Materials Letters, 2016, 185, 443-446.
17. Park, J. H. and Park, J. M., "Photo-generated cathodic protection performance of electrophoretically Co-deposited layers of TiO_2 nanoparticles and graphene nanoplatelets on steel substrate," Surface and Coatings Technology, 2014, 258, 62-71.
18. Lei, J., Shao, Q., Wang, X., Wei, Q., Yang, L., Li, H., Huang, Y. and Hou, B., "$ZnFe_2O_4$/TiO_2 nanocomposite films for photocathodic protection of 304 stainless steel under visible light," Materials Research Bulletin, 2017, 95, 253-260.
19. Han, C., Shao, Q., Lei, J., Zhu, Y. and Ge, S., "Preparation of NiO/TiO_2 p-n heterojunction composites and its photocathodic protection properties for 304 stainless steel under simulated solar light, Journal of Alloys and Compounds," 2017, 703, 530-537.
20. Liu, Y., Xu, C. and Feng, Z., "Characteristics and anticorrosion performance of Fe-doped TiO_2 films by liquid phase deposition method," Applied Surface Science, 2014, 314, 392-399.
21. Eslami, M., Hamnabard, Z. and Nemati, A., "Synthesis and spectral properties of Nd-doped glass-ceramics in SiO_2-CaO-MgO system prepared by sol-gel method," Journal of Rare Earths, 2013, 31, 595-599.
22. Tajer-Kajinebaf, V., Sarpoolaky, H. and Moham-

[DOI: 10.22068/ijmse.16.2.33]

madi, T., "Sol–gel synthesis of nanostructured titania–silica mesoporous membranes with photo-degradation and physical separation capacities for water purification," Ceramics International, 2014, 40, 1747-1757.
23. Alamolhoda, S., Mirkazemi, S. M., Shahjooyi, T. and Benvidi, N. "Effect of pH changes on phase constituents, microstructure and magnetic properties of nano-sized $NiFe_2O_4$ powder synthesized by sol–gel auto-combustion method," Iranian Journal of Materials Science and Engineering, 2016, 13, 21-27.
24. Shokuhfar, A., Alzamani, M., Eghdam, E., Karimi, M. and Mastali, S., "SiO2-TiO2 Nanostructure Films on Windshields Prepared by Sol-Gel Dip-Coating Technique for Self-Cleaning and Photocatalytic Applications, Nanoscience and Nanotechnology, 2012, 2, 16-21.
25. Yazdani, S., Javadpour, S., Mehdizadeh Naderi, S. and Javidi, M., "Corrosion resistant sol–gel coating on 2024-T3 aluminum, Iranian Journal of Materials Science and Engineering," 2016, 13, 44-49.
26. Huang, J., Shinohara, T. and Tsujikawa, S., "Effects of Interfacial Iron Oxides on Corrosion Protection of Carbon Steel by TiO₂ Coating under Illumination," Zairyo-to-Kankyo, 1997, 46, 651-661.
27. Shen, G. X., Chen, Y. C. and Lin, C. J., "Corrosion protection of 316 L stainless steel by a TiO_2 nanoparticle coating prepared by sol–gel method," Thin Solid Films, 2005, 489, 130-136.
28. M. G. Mahmoud, R. Wang, M. Kato, K. Nakasa, "Influence of ultraviolet light irradiation on corrosion behavior of weathering steel with and without TiO_2-coating in 3 mass% NaCl solution," Scripta Materialia, 2005, 53, 1303-1308.
29. Yu, J. and Zhao, X., "Effect of surface treatment on the photocatalytic activity and hydrophilic property of the sol-gel derived TiO_2 thin films," Materials Research Bulletin, 2001, 36, 97-107.
30. Yu, J., Zhao, X. and Zhao, Q., "Effect of film thickness on the grain size and photocatalytic activity of the sol-gel derived nanometer TiO_2 thin films," Journal of Materials Science Letters, 2000, 19, 1015-1017.
31. Wu, C. Y., Lee, Y. L., Lo, Y. S., Lin, C. J. and Wu, C. H., "Thickness-dependent photocatalytic performance of nanocrystalline TiO_2 thin films prepared by sol–gel spin coating," Applied Surface Science, 2013, 280, 737-744.
32. Pakma, O., Serin, N. and Serin, T., "The effect of repeated annealing temperature on the structural, optical, and electrical properties of TiO_2 thin films prepared by dip-coating sol–gel method," J. Mater Sci, 2009, 44, 401-407.
33. Karimi Sahnesarayi, M., Sarpoolaky, H. and Rastegari, S., "Evaluation of Crack-free Nanostructured Titania Coating Formation on Stainless Steel by Sol Gel Technique, in: 4th International Color and Coatings Congress, Tehran-Iran, 2011.
34. Swanepoel, R., "Determination of the thickness and optical constants of amorphous silicon," Journal of Physics E: Scientific Instruments, 1983, 16, 1214.
35. Kim, D. J., Hahn, S. H., Oh, S. H. ans Kim, E. J. "Influence of calcination temperature on structural and optical properties of TiO_2 thin films prepared by sol–gel dip coating," Materials Letters, 2002, 57, 355- 360.
36. Litter, M. I., Candal, R. J. and Meichtry, J. M. "Advanced oxidation technologies : sustainable solutions for environmental treatments," CRC Press/ Balkema, 2014, 192-193.
37. Curkovic, L., Curkovic, H. O., Salopek, S., Renjo, M. M. and Segota, S. "Enhancement of corrosion protection of AISI 304 stainless steel by nanostructured sol–gel TiO_2 films," Corrosion Science, 2013, 77, 176–184.
38. Park, H., Kim, K. Y. and Choi, W., "Photoelectrochemical Approach for Metal Corrosion Prevention Using a Semiconductor Photoanode," The Journal of Physical Chemistry B, 2002, 106, 4775-4781.
39. Li, S., Wang, Q., Chen, T., Zhou, Z., Wang, Y. and Fu, J., "Study on cerium-doped nano-TiO_2 coatings for corrosion protection of 316 L stainless steel," Nanoscale Research Letters, 2012, 7, 227-235.
40. Cao, G., Wang, Y., "Nanostructures and Nanomaterials: Synthesis", Properties, and Applications, World Scientific, 2011, 219-223.
41. Masalski, J., Gluszek, J., Zabrzeski, J., Nitsch, K. and Gluszek, P., "Improvement in corrosion resistance of the 316l stainless steel by means of Al_2O_3 coatings deposited by the sol-gel method," Thin Solid Films, 1999, 349, 186-190.
42. Yuan, J. and Tsujikawa, S., "Photo-Effects of Sol-Gel Derived TiO₂ Coating on Carbon Steel in Alkaline Solution," Zairyo-to-Kankyo, 1995, 44, 534-542.
43. Kanazawa, T. and Ohmori, "A. Behavior of TiO_2 coating formation on PET plate by plasma spraying and evaluation of coating's photocatalytic activity," Surface and Coatings Technology, 2005, 197, 45-50.

[DOI: 10.22068/ijmse.16.2.33]